Angewandte Chemie
Eine Zeitschrift der Gesellschaft Deutscher Chemiker

Supporting Information

Bioactive Macrocyclic Inhibitors of the PD-1/PD-L1 Immune Checkpoint

*Katarzyna Magiera-Mularz, Lukasz Skalniak, Krzysztof M. Zak, Bogdan Musielak, Ewa Rudzinska-Szostak, Łukasz Berlicki, Justyna Kocik, Przemyslaw Grudnik, Dominik Sala, Tryfon Zarganes-Tzitzikas, Shabnam Shaabani, Alexander Dömling, Grzegorz Dubin, and Tad A. Holak**

anie_201707707_sm_miscellaneous_information.pdf

Supporting Information

Table of Contents

Experimental Procedures

Antibodies and peptides targeting PD-1/PD-L1 checkpoint

The following therapeutic antibodies were used: durvalumab (anti-PD-L1; MEDI4736, trade name: Imfinzi, AstraZeneca Pharmaceuticals), and nivolumab (anti-PD-1; MDX-1106, trade name: Opdivo, Bristol-Myers Squibb).

The peptides were selected from the example peptides provided in the US patent 20140294898 and synthesized in-house (peptide-57 and -99) or by a commercial vendor (peptide-71; Bachem).

Protein expression and purification

Expression and purification of human PD-L1 (residues 18-134, C-terminal His-tag) were carried out essentially as described previously [1]. In brief, the *E. coli* strain BL21 were cultured at 37^{o}C until OD_{600nm} has reached 1.0, induced with 1 mM IPTG and cultured for additional 5 h. Inclusion bodies were collected by centrifugation, washed twice with 50 mM Tris-HCl pH 8.0 containing 200 mM NaCl, 0.5% Triton X-100, 10 mM EDTA and 10 mM 2-mercaptoethanol and once with the same buffer without the detergent. The inclusion bodies were dissolved by stirring overnight in 50 mM Tris pH 8.0 containing 6M GuHCl, 200 mM NaCl and 10 mM 2-mercaptoethanol. Solubilized fraction was clarified by high speed centrifugation. Protein was refolded by drop-wise dilution into 0.1 M Tris pH 8.0 containing 1 M L-Arg hydrochloride, 0.25 mM oxidized glutathione and 0.25 mM reduced glutathione. After refolding, the protein was concentrated, dialyzed 3 times against 10 mM Tris pH 8.0 containing 20 mM NaCl, and purified by size exclusion chromatography on Superdex 75 (GE Healthcare) in 10 mM Tris pH 8.0 containing 20 mM NaCl. The purity and protein folding were evaluated by SDS-PAGE and NMR, respectively.

Nuclear magnetic resonance (NMR) interaction assay

Uniform ^{15}N labelling was obtained by expressing the protein in the M9 minimal medium containing $^{15}NH_4Cl$ as the sole nitrogen source. For NMR measurements the buffer was exchanged by gel filtration to PBS pH 7.4. 10% (v/v) of D_2O was added to the samples to provide lock signal. All spectra were recorded at 300K using a Bruker Avance III 600 MHz spectrometer. Binding of tested ligands was analyzed by titrating the ^{15}N-labeled PD-L1 (0.2 mM) and recording the changes in the ^{15}N HMQC spectra during addition of the ligand.

Differential scanning fluorimetry (DSF) assay

The DSF analysis was carried out according to the procedure of Niesen *et al*, (2007). In brief, PD-L1 (12.5 μM) was incubated alone, or with peptide-57, or peptide-71 (both 25 μM) in the presence of the SYPRO Orange Dye (Life Technologies). A constant temperature gradient of 0.2°C/min was applied and changes in the fluorescence were monitored using a real time thermocycler (BioRad). Melting temperature (Tm) was estimated from the first derivative of the fluorescence intensity as a function of temperature.

Cell based PD-1/PD-L1 interaction functional assay

For the assay, two genetically modified cell lines were used: a surrogate of antigen-presenting cells (PD-L1 aAPC/CHO-K1 cell line overexpressing an activating TCR ligand and PD-L1, referred further as APC cells), and a surrogate of T cells (Jurkat T cells carrying the luciferase reporter under the control of NFAT promoter and overexpressing PD-1, called PD-1 Effector Cells). The cells were purchased from

Promega and cultured in RPMI 1640 medium (Lonza) supplemented with 10% Fetal Bovine Serum (BioWest), 100 U/ml Penicillin and 100 U/ml Streptomycin. Before the experiments both cell lines were propagated in a constant presence of Hygromycin B (50 µg/ml) and G418 (250 µg/ml) to provide a stable presence of the introduced genetic constructs. The overexpression of PD-1 and PD-L1 was confirmed by flow cytometry. The cells were periodically tested and found negative for Mycoplasma contamination using PCR-based method [3].

APC cells were seeded at 10,000 cells per well in 96-well plates 20 h prior to the assay. On the day of the assay serial dilutions of tested macrocyclic peptides and control antibodies were prepared in the culture medium and added to the wells containing APC cells. Since stock solutions of peptides were prepared in DMSO, care was taken to keep the concentration of DMSO constant and below observable influence on the test results. Immediately after the addition of tested compounds 20,000 PD-1 Effector Cells were added in the same medium. The cells were incubated for 6 hours and equilibrated for 30 min at room temperature. Bio-Glo reagent (Promega) was added and the luminescence was determined after further 20 min incubation. Half maximal effective concentrations (EC_{50}) and maximal luminescence values (RLU_{max}) were determined by fitting the Hill equation to the experimental data.

Crystallization of the hPD-L1/peptide complexes

PD-L1 was prepared in 10 mM Tris-HCl pH 8.0 containing 20 mM NaCl and concentrated to 5 mg/ml. Peptides were added at 1:3 molar ratio (protein:peptide) just prior to crystallization. Screening was performed using a sitting-drop vapor diffusion method and commercially available sets of conditions (Hampton Research,

Emerald Biosciences). Diffraction-quality crystals were obtained at room temperature from 0.2 M ammonium acetate (pH 5.5) containing 0.1 M Bis-Tris and 25% PEG 3350 for the hPD-L1/peptide-57 complex and from 0.2 M imidazole malate (pH 8.5) containing 27% PEG 10 000 for the of hPD-L1/peptide-71 complex.

Structure solution and refinement

The X-ray diffraction data were collected on beamline BL14.1 operated by Helmholtz-Zentrum Berlin (HZB) at BESSY II (Berlin, Germany).[4] The data collected for peptide-57 complex were indexed and integrated using MOSFLM and scaled using SCALA[5] contained in CCP4 package. The data for peptide-71 complex were indexed, integrated, and scaled using XDS[6] package with XDSAPP2.0 GUI.[7] Molecular replacement was calculated using Phaser[8,9] and PDB ID 5C3T as a search model. Structures were built using Coot[10,11] and refined using Refmac[12] or Phenix.[13] Water molecules were added automatically and inspected manually. Rfree was used to monitor the refinement strategy. Models were validated using the Molprobity.[14]

Coordinates and structure factors were deposited in the Protein Data Bank with accession numbers 5O4Y (hPD-L1/peptide-57) and 5O45 (hPD-L1/peptide-71).

Peptide synthesis

All reagents and solvents were purchased from Sigma-Aldrich, Iris Biotech, Merck or Bachem and used without further purification. Linear peptides with chloroacetic acid at N-terminus were obtained with an automated solid-phase peptide synthesizer (Biotage® Initiator+Alastra™) using rink amide AM resin (loading: 0.59 mmol/g). Fmoc deprotection was achieved using 20% piperidine in DMF for 3 + 10 min. A

double-coupling procedure was performed with 0.5 M solution of DIC (5 eq.) and 0.5 M solution of OXYMA (5 eq.) and 0.1 M Fmoc-protected amino acid (5 eq.) in DMF, 2 x 15 min at 75 ^{o}C for all amino acids with the exception of amino acids following N-methylated residues. Amino acid after N-methylated residues were also double coupled using 0.5 M solution of DIC (5 eq.) and 0.5 M solution of OXYMA (5 eq.) and 0.1 M Fmoc-protected amino acid (5 eq.) in DMF, 2 x 15 min at 75 ^{o}C and second coupling was extended for 6h at room temperature. After this extended double coupling procedure the non-reacted peptide was acetylated (Ac_2O, DIPEA, 15 eq., 15 min. at room temperature). N-Terminal chloroacetic acid was also double-coupled with 0.5 M solution of DIC (5 eq.) and 0.5 M solution of OXYMA (5 eq.) and 0.1 M chloroacetic acid (5 eq.) in DMF, 2 x 15 min at 75 ^{o}C. Cleavage and deprotection of the linear peptides from the resin was accomplished with the mixture of TFA/tioanisole/EDT/anisole (90:5:3:2) after 3 h of shaking. The crude peptide was precipitated with ice-cold diethyl ether and centrifuged (9 500 rpm, 3 x 8 min, 4 °C). Peptides were dried in stream of argon. Cyclization procedure: peptide was dissolved in acetonitrile/0.1 M ammonium carbonate buffer pH 8.5 (1:2, v/v) and mixture was stirred for 24h. The solution was evaporated *in vacuo* to obtain solid residue. Peptides were purified using preparative HPLC (Knauer Prep) with a C18 column (Thermo Scientific, Hypersil Gold 12 µm, 250 mm x 20 mm) with water/acetonitrile (0.05% TFA) eluent system. Analytical HPLC was done using the Kinetex 5 µm EVO C18 100A 150 x 4.6 mm column or the Waters C18 1.7 µm 50 mm x 2.1 mm column.

Peptide **57**: t_R = 30.1 min, prep HPLC, gradient: 0 min, 25% B, 5 min 25% B, 50 min. 75% B, 52 min 95% B, 55 min. 90% B, 60 min. 25% B; t_R = 9.55 min, anal. HPLC, gradient: 0 min. 25% B, 2 min 25% B, 13 min 75% B, 15 min, 25% B; HR ESI-MS: found 934.9769 ($M+2H^+/2$), expected 934.9767.

Peptide **99**: t_R = 21.05 min, prep HPLC, gradient: 0 min, 20%B, 5 min 20% B, 45 min, 60 % B, 47 min 90% B, 50 min, 90% B, 55 min, 20 % B; t_R = 7.39 min, anal. HPLC, gradient: 0 min. 25% B, 2 min 25% B, 13 min 65% B, 15 min, 25% B; HR ESI-MS: found 816.9614 ($M+2H^+/2$), expected 816.9619.

Results and Discussion

Structural basis of PD-L1 interaction with peptide-71

High quality crystals of the complex of the distal IgG domain of PD-L1 and the full-length peptide-71 were obtained, which allowed solving the structure at below 1 Å resolution. The structure contains one protein molecule and one molecule of the macrocyclic peptide-71 in the asymmetric unit. Both molecules are well defined by their respective electron densities (Figure 2A and Supporting Information, Figure S5A). The domain of PD-L1 folds into an 11-stranded β sandwich stabilized by a single disulphide bond characteristic of the IgG-like domains. The domain is appended with a linker and 6-histidine tag added in cloning which are both well defined by their respective electron densities by virtue of their stabilizing interaction with the adjacent PD-L1 molecule within the crystal lattice.

Peptide-71 binds PD-L1 at the hydrophobic palm of the β-sheet sandwich of PD-L1 (Figure 2B and Supporting Information, Figure S7), exactly at the site of the PD-1 interaction (Figure 3A-C), providing rationale for the inhibitory role of peptide-71. The β-sheet is composed of strands G, F, C and C' with the peptide ring plane parallel to the plane of the β-sheet (Figure 4, Supporting Information, Figures S7, S9 and S10; the canonical Ig-strand designations are used – Figure S14).

The peptide itself has a ring like shape, while its centre is filled with the hydroxyphenyl moiety of $_{71}$Tyr11 (the subscript indicates peptide-71) and the entire

peptide wraps around this central aromatic ring. The toroidal part of the macrocycle is composed primarily of the mainchain atoms and the ring closing cysteine side chain. The backbone is extended in the region of $_{71}$Tyr11-$_{71}$Scc13 and directly adjacent $_{71}$Phe1-$_{71}$NMeNle3 and forms three consecutive β-turns between $_{71}$NMeNle3-$_{71}$Trp10, stabilized by hydrogen bonds between $_{71}$NMeNle3 carbonyl and $_{71}$Val6 amine, $_{71}$Asp5 carbonyl and $_{71}$Tyr8 amine, and $_{71}$NMePhe7 carbonyl and $_{71}$Trp10 amine. The sidechains decorate the ring such that all polar group containing moieties are located above the ring plane while the majority of hydrophobic moieties are exposed below the ring plane which makes the entire structure amphipathic.

The hydrophobic side of the ring is directed towards PD-L1 and contributes the majority of the interactions (Figure 4) while the hydrophilic side is exposed to the solvent. Such binding resembles one of the two likely binding modes of macrocycles, the “face-on binding”, according to the nomenclature proposed by.[15] Such binding mode creates a large surface of interaction burying approximately 1107 Å^2.

The binding surface of the peptide may be divided into two major zones dominated by interactions of different physicochemical character. The hydrophobic zone is dominated by three aromatic moieties ($_{71}$Phe1, $_{71}$NMePhe7, $_{71}$Trp10) supplemented with $_{71}$NMeNle3 and $_{71}$Val6. The sidechains of the four former residues bind within a relatively hydrophobic cleft at the PD-L1 surface located perpendicular to the sheet forming the G, F, C, C’ β-sheet. Of particular interactions, the sidechain of $_{71}$Phe1 is involved in π-π stacking with the sidechain of Tyr65. The pocket accommodating $_{71}$Phe1 is completed by intermolecular interactions with $_{71}$NMeNle3, $_{71}$NMePhe7. The former residue sits in a shallow cleft formed by the sidechains of Ile54 and Val68, but also Gln66 and Asp73. The latter forms alkyl-π interaction with the sidechain of Met115 while sitting in a pocket completed by the sidechains of

Ile54, Ser117, Ala121 and Tyr56 and also $_{71}$Val6 and $_{71}$Trp10. The latter residue is stabilized by T stacking with Tyr123 and sits in a shallow pocket completed by Ala121 and Met115 (Figure 4B and Supporting Information, Figure S10). The sidechain of $_{71}$Val6 forms hydrophobic interactions at the rim of the cleft with the sidechain of Ile54.

The polar zone of the interaction surface is located at its periphery and includes two short (~2.8 Å) hydrogen bonds contributed by backbone amines of $_{71}$Leu12 and $_{71}$Scc13 with the sidechain carboxyl of Glu58. Additionally, within the macrocycle forming structure, the sulphur atom of $_{71}$Scc13 interacts with backbone carbonyl of Asp61 and a hydrogen bond connects backbone carbonyl N-terminal to $_{71}$Phe1 with the sidechain amine of Asn63 (Figure 4C). Further, carbon hydrogen bonds and water mediated interactions stabilize the binding in this region.

Overall, the interaction surface of peptide-71 and PD-L1 is relatively large and flat. As such, the affinity is guided by multiple low energy interactions rather than dominated by any pronounced pockets. Such interaction at shallow pockets of a relatively flat protein surface is characteristic for the binding of macrocyclic peptides as previously noted by Villar and colleagues.[15]

The surface of the macrocyclic peptide-71 distal to the protein molecule is decorated with a number of polar groups providing favourable solvation. These include the sidechains of $_{71}$Asp5, $_{71}$Tyr8 and $_{71}$Gly-$NH_2$14, and a number of carbonyl moieties within the mainchain. However, two regions within the peptide are poorly organized in this regard. The $_{71}$NMePhe2 hydrophobic sidechain is exposed directly to the solvent. Further, a large hydrophobic patch is exposed around $_{71}$Val6 and $_{71}$NMeNle3 which could afford additional modification by incorporation of unnatural, amphipathic sidechains.

Structure of the PD-L1/peptide-57 complex

The structure was solved at the 2.5 Å resolution and the structural model is characterized by reasonable geometry and explains the experimental data at acceptable level (Table S2). The asymmetric unit contains three protein molecules (distal domains of the extracellular part of PD-L1) and three 57 peptides each in the vicinity of different protein molecule. All the molecules are well defined by their respective electron densities (Supporting Information, Figure S5B) save only for the 6 histidine tag used for protein purification.

The structures of all three PD-L1 domains contained in the asymmetric unit are virtually identical to each other and to the structure of PD-L1 in complex with peptide-71 (average rmsd = 0.42 Å). The binding area of macrocyclic peptide-57 at the surface of PD-L1 is comparable to that of peptide-71 (Supporting Information, Figures S6 and S8), however the peptide disposition and the majority of the interactions are dissimilar. The backbone of peptide-57 assumes an elliptic shape with a bulge flapped over the central region.

The ellipse is composed of the backbone atoms which also form a bulge at the middle of the longer axis which flaps over the central region. The bulge is stabilized by a hydrogen bond contributed by $_{57}$Phe1 amine and $_{57}$Arg13 carbonyl and as such is reminiscent of a β-turn, however the turn extends through the cyclizing $_{57}$Scc14 sidechain which formally precludes such classification. This structure is directly preceded by another turn ($_{57}$Phe1-$_{57}$Asn3) reminiscent of β-turn, but again containing a fragment of the moiety introduced for cyclization. The backbone spanning residues $_{57}$His5-$_{57}$Trp10 is extended while residues at its beginning and end form wide turns completing the ellipsoid. The flap is located above the ellipse plane and decorated

mostly by polar moieties containing sidechains. Below the ring plane, the backbone is decorated with hydrophobic sidechains extending roughly 45° to the ring plane. Such composition renders the entire structure amphipathic.

The ellipse plane of peptide-57 is parallel to the plane of G, F, C and C' β-sheet (Supporting Information, Figures S11-S13). The macrocycle exhibit face-on binding with hydrophobic face of the peptide molecule contributing the majority of the interactions with PD-L1 and the polar face being exposed to the solvent. The interaction is spatially extended with the buried surface area of 1230 $Å^2$.

The binding of peptide-57 may be divided into dominant hydrophobic zone and smaller polar zone. Within the hydrophobic zone three aromatic moieties ($_{57}$Phe1, $_{57}$Trp8 and $_{57}$Trp10) and two large hydrophobic sidechains ($_{57}$NMeNle11 and $_{57}$NMeNle12) dominate the interaction while further hydrophobic contacts are contributed by $_{57}$Pro4. Two major hydrophobic pockets at the surface of PD-L1 are filled with indole moieties of $_{57}$Trp8 and $_{57}$Trp10. The first pocket is constituted by the sidechains of Ile54, Tyr56, Gln66 and Val68, with the sidechain of Tyr56 providing a T-stacking interaction whereas that of Gln66 a pronounced aliphatic-π interaction. $_{57}$Trp10 accommodating pocket is composed of Tyr56, Glu58, Arg113, Met115 and Tyr123 sidechains (Supporting Information, Figures S11B, S12 and S13). Both Tyr residues provide stacking interactions with the imidazole ring, while Arg, Met and to a lesser extent Glu provide alkyl-π contributions. The two norleucine sidechains provide a lid over Met115. Additionally, $_{57}$Nle11 closes the $_{57}$Trp10 pocket through week interaction with Tyr123 whereas $_{57}$NMeNle12 provides week interaction with Ala121 and intermolecular interaction with $_{57}$Phe1 sidechain. The latter sidechain binds weakly at Ile54. The ring of $_{57}$Pro4 anchors weakly at the sidechain of Val68.

The polar contribution to the binding of peptide-57 at the surface of PD-L1 encompasses two hydrogen bonds contributed by backbone carbonyl of $_{57}$Leu6 and backbone amide $_{57}$Trp8 and the sidechain of Gln66. In the close vicinity, Asn63 sidechain contributes a hydrogen bond to backbone carbonyl of $_{57}$Trp8 (Figure S11C).

Overall, the interaction of macrocyclic peptide-57 with PD-L1 is guided by hydrophobic interactions of indole sidechains located in the central part and along the long axis of the molecule at respective subpockets which binding is supplemented by a number of weak hydrophobic interactions at one of the long rims of the molecule and polar binding along the other long rim. The interaction surface corresponds to the binding site of PD-1 providing rationale for inhibitor function of macrocyclic peptide-57.

The solvent exposed surface to the macrocyclic peptide-57 is decorated with polar sidechains including $_{57}$Asn3, $_{57}$His5, $_{57}$Ser7, $_{57}$Arg13 and $_{57}$Gly-$NH_2$15. Together with the exposed polar groups within the backbone these moieties provide favourable solvent contacts, although $_{57}$Leu6 sidechain is also entirely directed towards the solvent. Further, the sidechains of $_{57}$Phe1, $_{57}$NMeAla2, $_{57}$Pro4, $_{57}$NMeNle11 and $_{57}$NMeNle12 are not entirely buried within protein structure but rather lie on its surface covering the hydrophobic patch at the PD-L1 binding site but at the same time exposing hydrophobic surface of their aromatic/aliphatic sidechains.

Detailed comparison of interactions in PD-L1/peptide-57 and PD-L1/peptide-71 complexes

Peptide-57 exposes two parallel stretches of hydrophobic sidechains ($_{57}$Phe1-$_{57}$NMeNle11-$_{57}$NMeNle12 and $_{57}$Pro4-$_{57}$Trp8-$_{57}$Trp10) which bind at the surface of PD-L1 at an angle of about 30° relative to the direction of G, F, C, C' strands. In turn

the hydrophobic region of interaction in peptide-71 is composed of a zigzag of sidechains ($_{71}$Phe1, $_{71}$NMePhe7, $_{71}$Trp10) almost perpendicular to the direction of PD-L1 strands. It follows, that the particular interactions are also largely different. The binding landscape of peptide-57 is dominated by two significant pockets accommodating bulky indole sidechains covered with the lid accommodating further nonpolar residues. The binding landscape of peptide-71 is in turn characterized by a single significant hydrophobic pocket accommodating the sidechain of $_{71}$NMePhe6 whereas the rest of the nonpolar interactions are more superficial.

Unlike within the region of hydrophobic interactions, the dispositions of all involved PD-L1 polar residues differ between the structures. Although the main chains overlay almost perfectly in the discussed region and the differences concern only the sidechains their extent affects the entire PD-L1 landscape at the binding site involving Glu58, Asp61, Asn63 and Arg113. Peptide-57 anchors primarily at Asn63 and Gln66 whereas peptide-71 at Glu58 and Asn63 and further significant interaction is provided by the mainchain carbonyl of Asp61 and the cyclizing sulphur atom. In peptide-57 the cyclizing sulphur is distant form the interaction surface.

Table S1. The IC_{50}'s of the PD-1/PD-L1 interaction for representative macrocyclic peptides containing 15, 14 and 13 residues.

Complex	**Affinity nM**	**Reference**
Human PD-1/human PD-L1	Kd 8000.2 ± 0.1	Cheng et al, 2013;[16] Lin et al. 2008[17]
Peptide-57	IC_{50} 9	Miller et al, 2014[18]
Peptide-71	IC_{50} 7	Miller et al, 2014[18]
Peptide-99	IC_{50} 153	Miller et al, 2014[18]
PD-1 / nivolumab	Kd 1.45- 4.03	Tan et al, 2017b[19]
PD-1 / pembrolizumab	Kd 0.027	Na et al, 2017[20]
PD-L1 / BMS-936559	Kd 0.830	Tan et al, 2017a[21]
PD-L1 / avelumab	Kd 0.042	Liu et al, 2017[22]

Table S2. Data collection and refinement statistics (molecular replacement)

	PD-L1 in complex with peptide-57	PD-L1 in complex with peptide-71
Data collection		
Wavelength (Å)	0.9184	0.9184
Space group	P 1 21 1	P 21 21 21
Cell dimensions		
a, b, c (Å)	50.55 80.95 54.23	31.81, 53.68, 80.93
α, β, γ (°)	90 104.49 90	90, 90, 90
Resolution range (Å)	28.92 - 2.3 (2.382 - 2.3)*	44.73 - 0.99 (1.025 - 0.99)*
R_{merge}	0.107 (0.552)	0.033 (0.887)
$I/\sigma I$	6.6 (2.1)	19.7 (1.9)
Completeness (%)	97.87 (98.61)	94.3 (90.4)
Redundancy	3.0 (3.2)	6.7 (6.5)
Total reflections	56472	490522
CC1/2	0.992 (0.623)	0.998 (0.723)
Refinement		
Resolution (Å)	2.3	0.99
No. reflections	18509 (1843)	73554 (6965)
R_{work}/R_{free}	0.1977/ 0.2622 (0.3125/0.4367)	0.1123/0.1367 (0.2043/0.2191)
Wilson B-factor	36.17	9.87
No. atoms	3209	1669
Protein	2706	1162
Ligand	398	129
Water	105	378
Ramachandran favoured (%)	93.10	93.70
Ramachandran allowed (%)	6.61	6.30
Ramachandran outliers (%)	0.29	0.00
B-factors	43.57	17.89
Protein	43.32	13.24
Ligand	46.04	11.82
Water	40.58	34.25
R.m.s deviations		
Bond lengths (Å)	0.013	0.020
Bond angles (°)	2.05	1.75

*Values in parentheses are for highest-resolution shell.

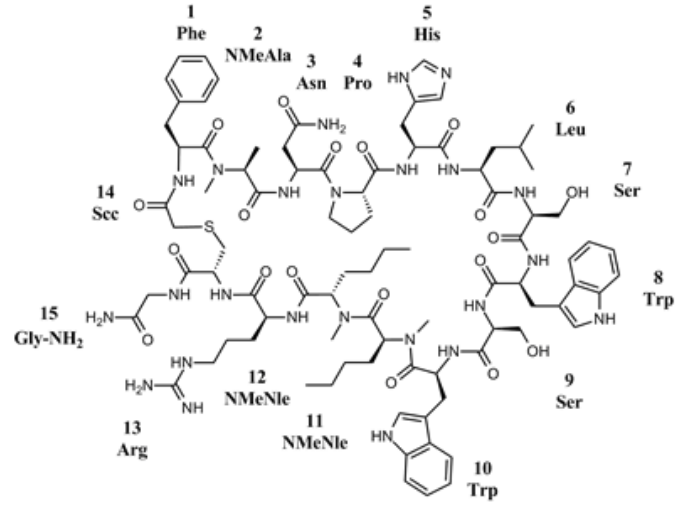

peptide 57

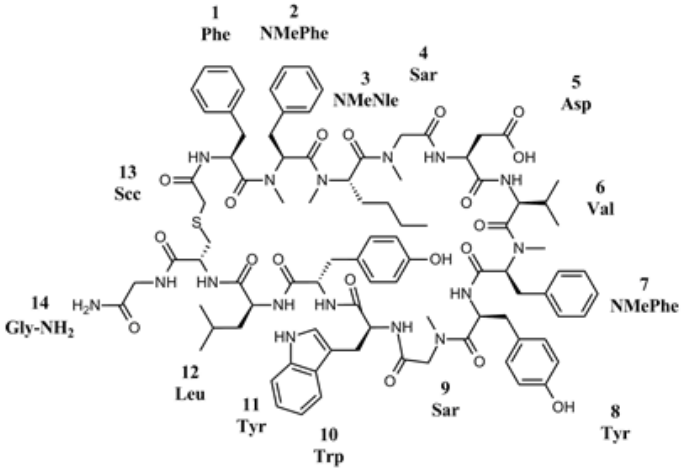

peptide 71

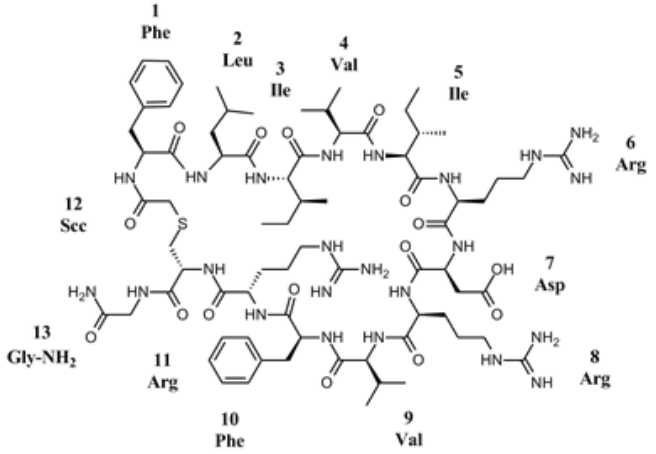

peptide 99

Figure S1. Chemical structures of macrocyclic peptides-57, -71 and -99. Compound numbering according to the patent application US 20140294898 A1.[14]

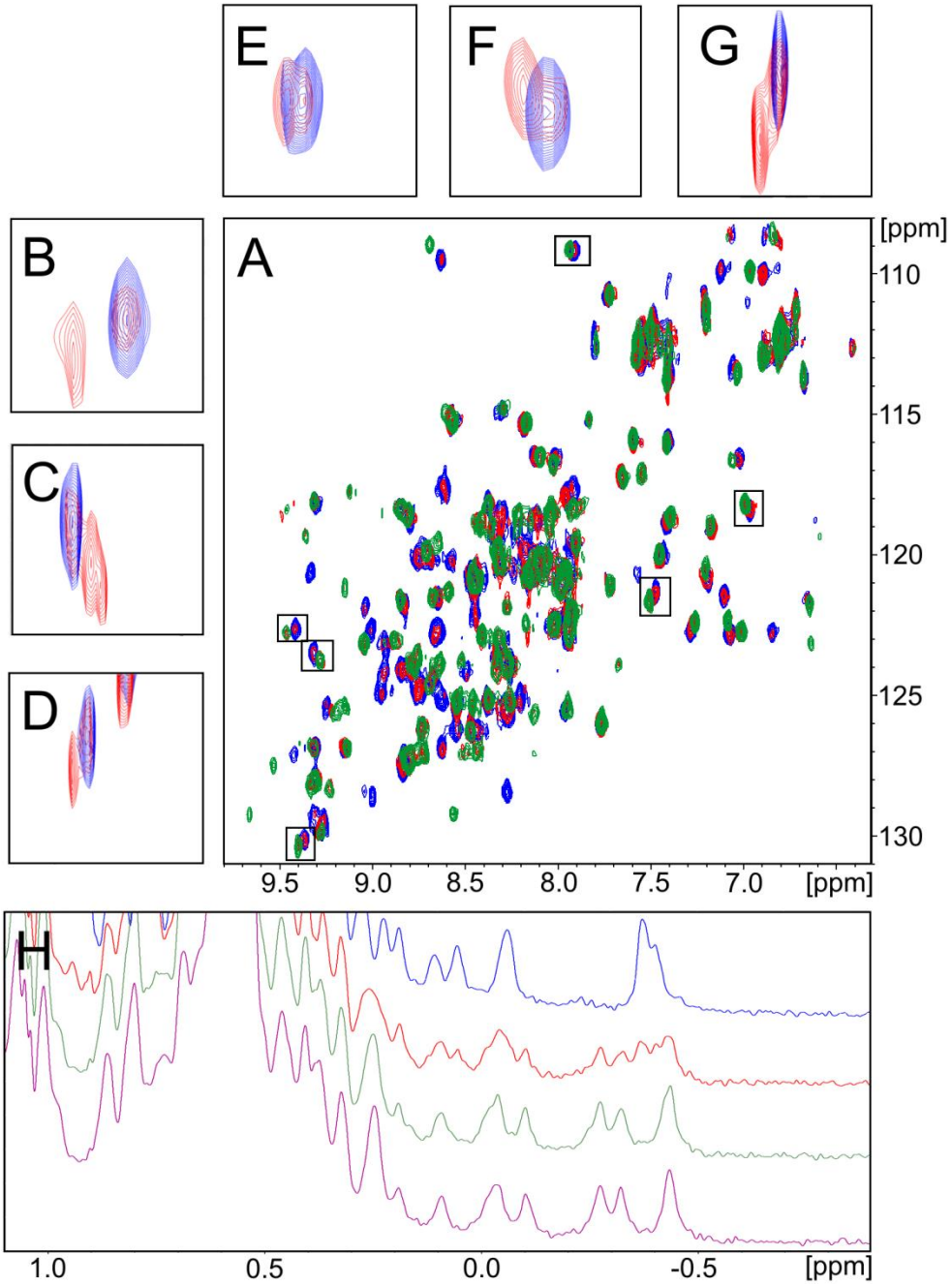

Figure S2. Titration of PD-L1 with peptide-71 monitored by the NMR method.

A constant amount of the ^{15}N labeled protein was titrated with increasing concentrations of tested compounds while monitoring the ^{1}H-^{15}N signals in 2D HMQC NMR spectra. A) The ^{1}H-^{15}N HMQC spectrum for the ^{15}N labeled PD-L1 with peptide-71. Blue - reference PD-L1, red - the PD-L1/peptide-71 in the molar ratio 5/1, green – the PD-L1/peptide-71 in the molar ratio 1/1, respectively. B)-G) Enlargements of the insets in spectrum A) showing resonance the peak doubling. H) ^{1}H NMR spectra for the titration of PD-L1 with peptide-71. Blue: the reference apoPD-L1; red – the PD-L1/peptide-71 in the molar ratio 7/1, green – 5/1, and 1/1, respectively.

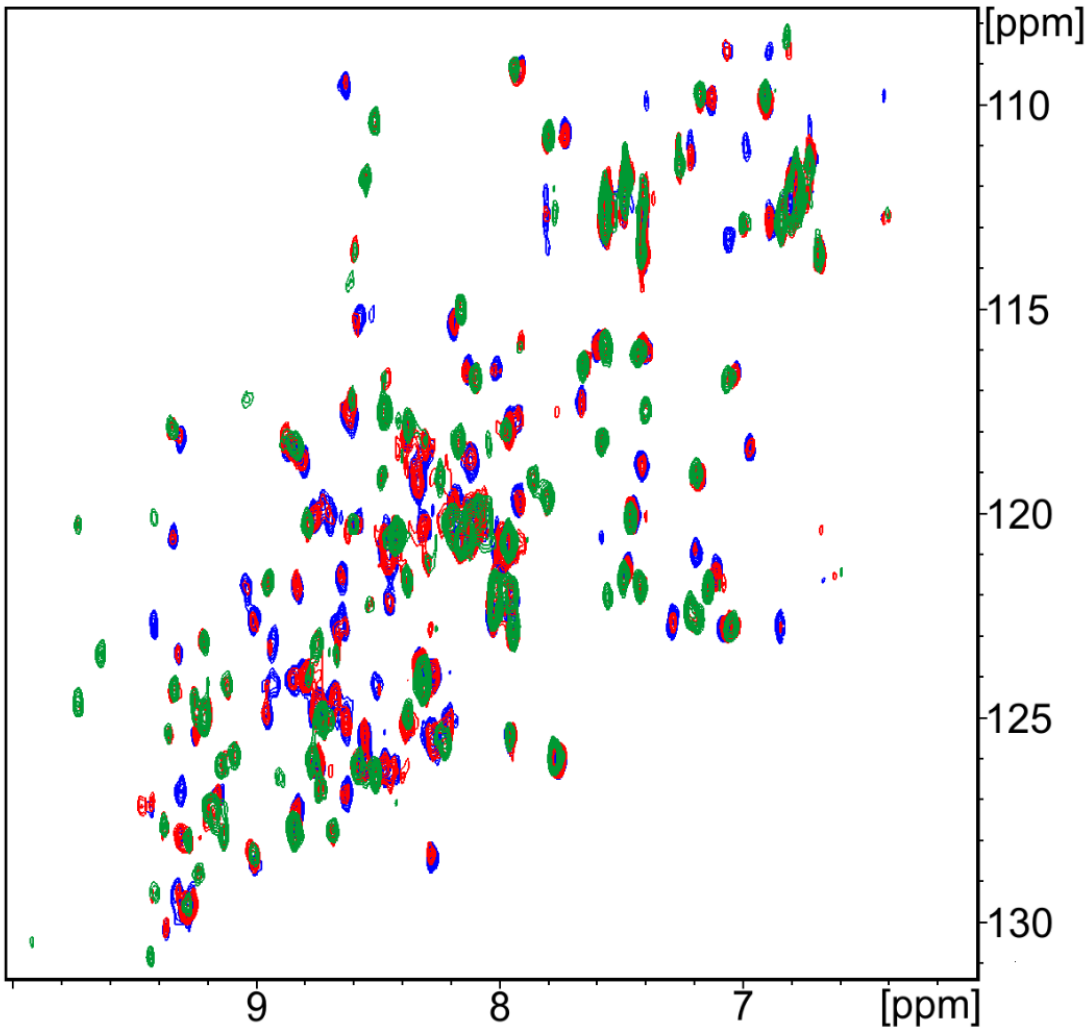

Figure S3. ^{1}H-^{15}N HMQC spectra of the ^{15}N labeled PD-L1 titrated with peptide-57. Blue - reference PD-L1, red - the PD-L1/peptide-57 in the molar ratio 4/1, green - the PD-L1/peptide-57 in the molar ratio 1/1, respectively.

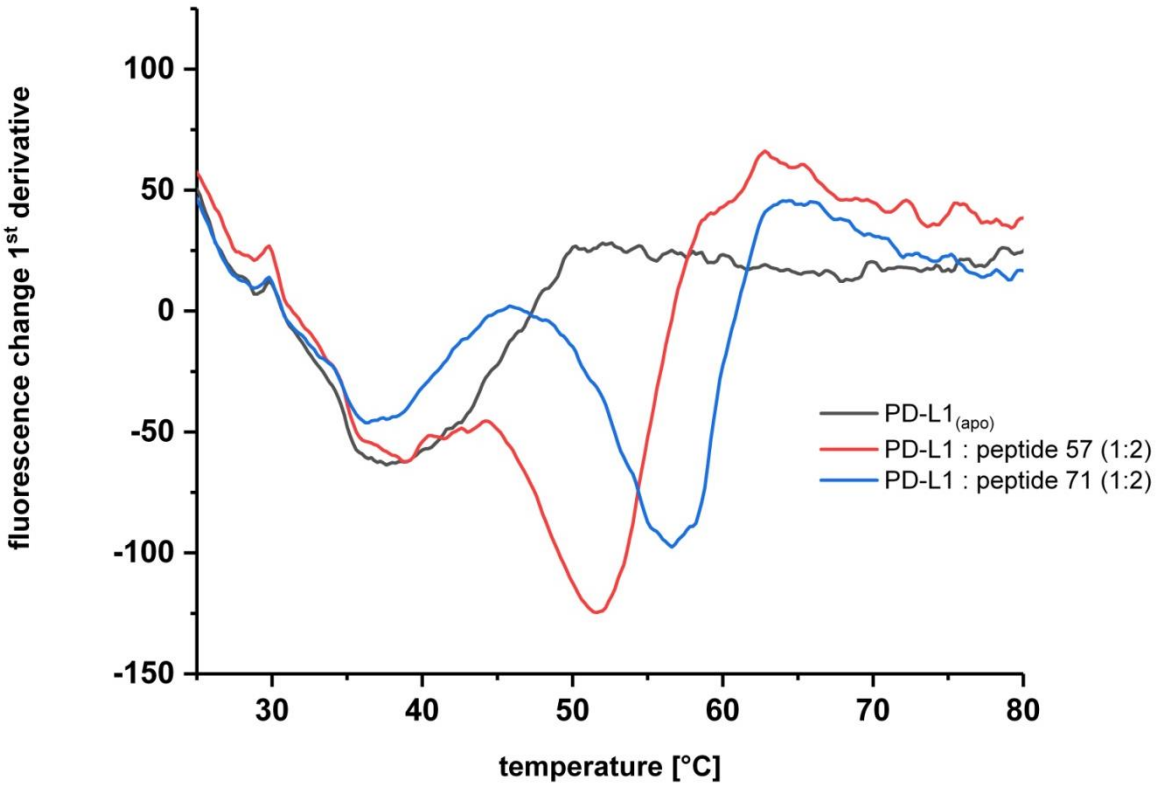

Figure S4. Peptides-57 and -71 induce thermal stabilization of PD-L1. Thermal unfolding of the protein was monitored by the DSF. First derivatives of temperature dependence of the fluorescence intensity are shown. A significant compound induced shift in melting temperature is observed for both peptides. Black – reference PD-L1, red the PD-L1/peptide-57 in the molar ratio 1:2, blue - the PD-L1/peptide-71 in the molar 1:2.

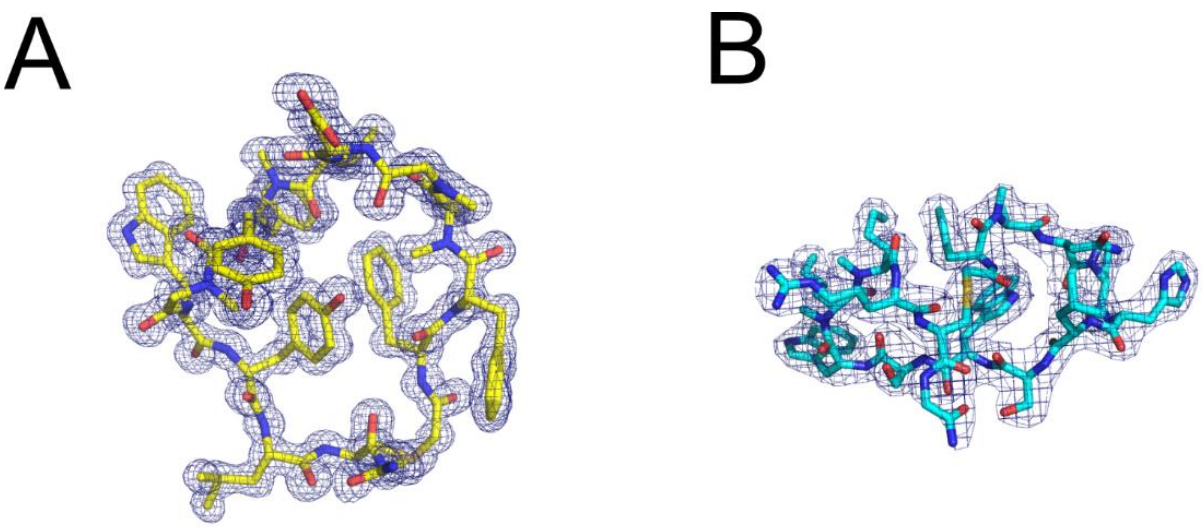

Figure S5. Quality of the electron density map for the peptide structures of the A) PD-L1/peptide-71 and B) PD-L1/peptide-57 complex. Examples of the 2Fo-Fc maps show a continuous, well interpretable electron density that defines the peptide inhibitors.

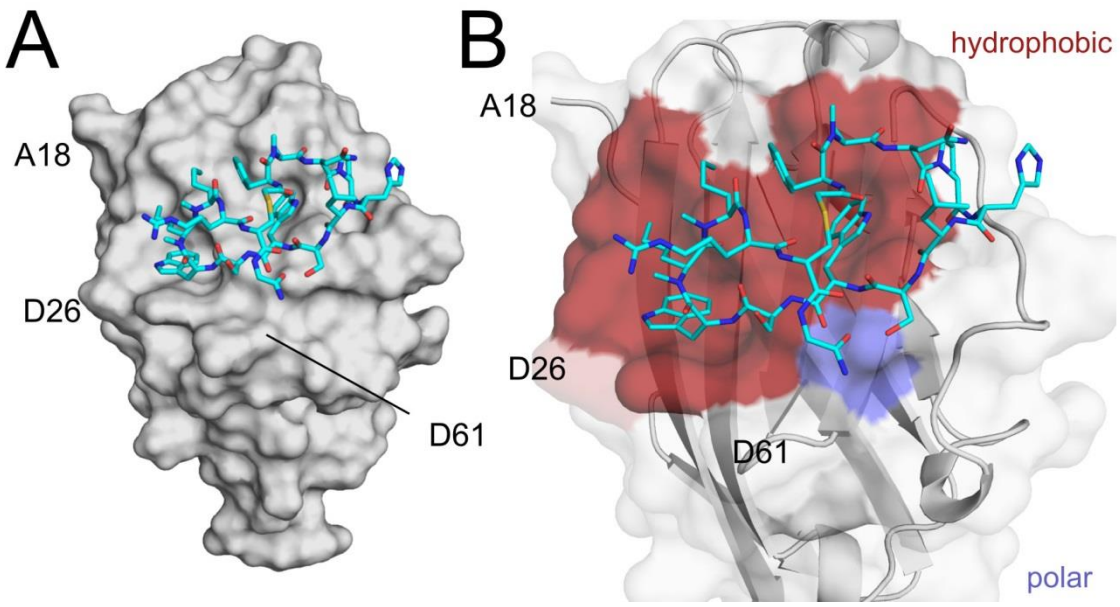

Figure S6. Crystal structure of the PD-L1/peptide-57 complex. A) Overall view into the PD-L1/peptide-57 interaction. Peptide-57 assumes an elliptic shape with a bulge flapped over the central region of the peptide. B) A close-up view of the PD-L1/peptide-57 interface. Peptide-57 binds on the surface of PD-L1 at the relatively hydrophobic palm. Hydrophobic interactions in the complex are presented in red while hydrophilic in blue.

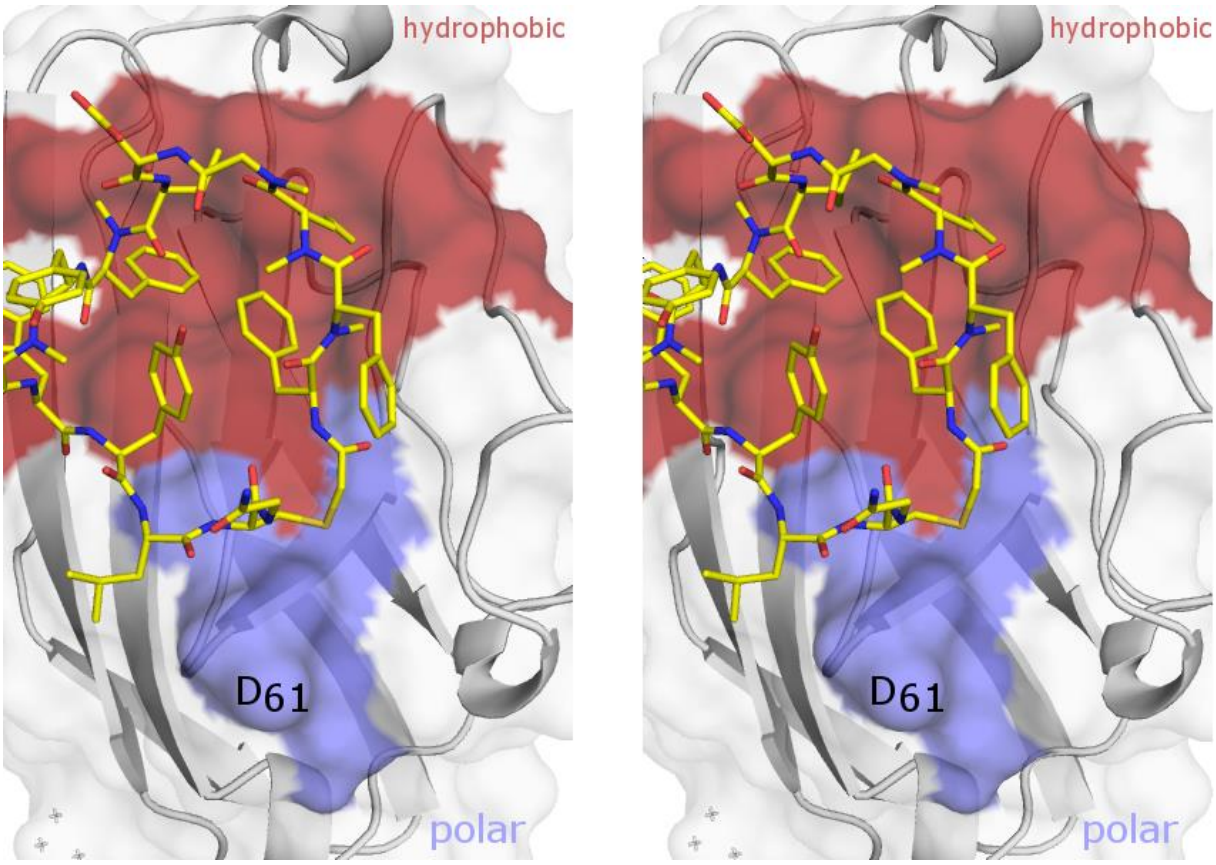

Figure S7. Close-up stereoview of the PD-L1/peptide-71 interface. Hydrophobic interactions in the complex are shown in red, while hydrophilic in blue.

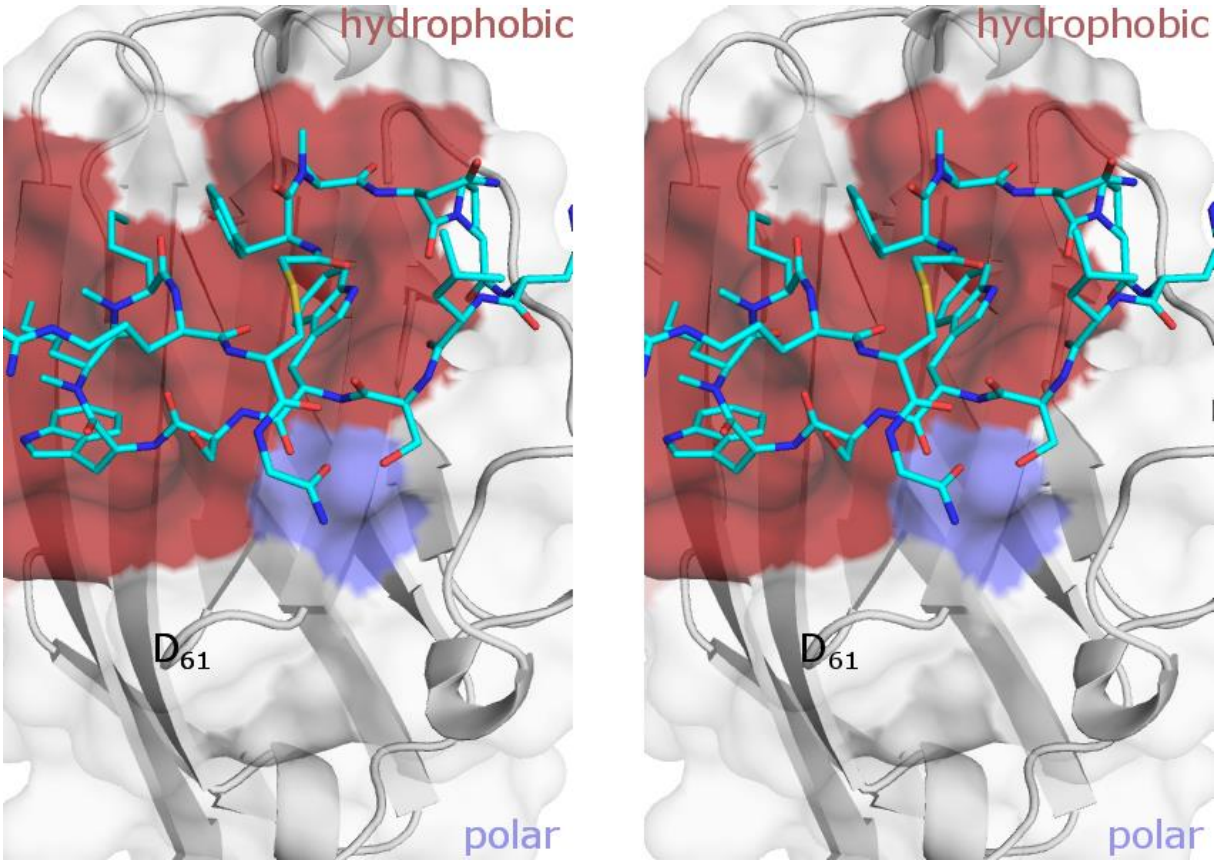

Figure S8. The close-up stereoview of the PD-L1/peptide-57 interface. Hydrophobic interactions in the complex are presented in red, while hydrophilic in blue.

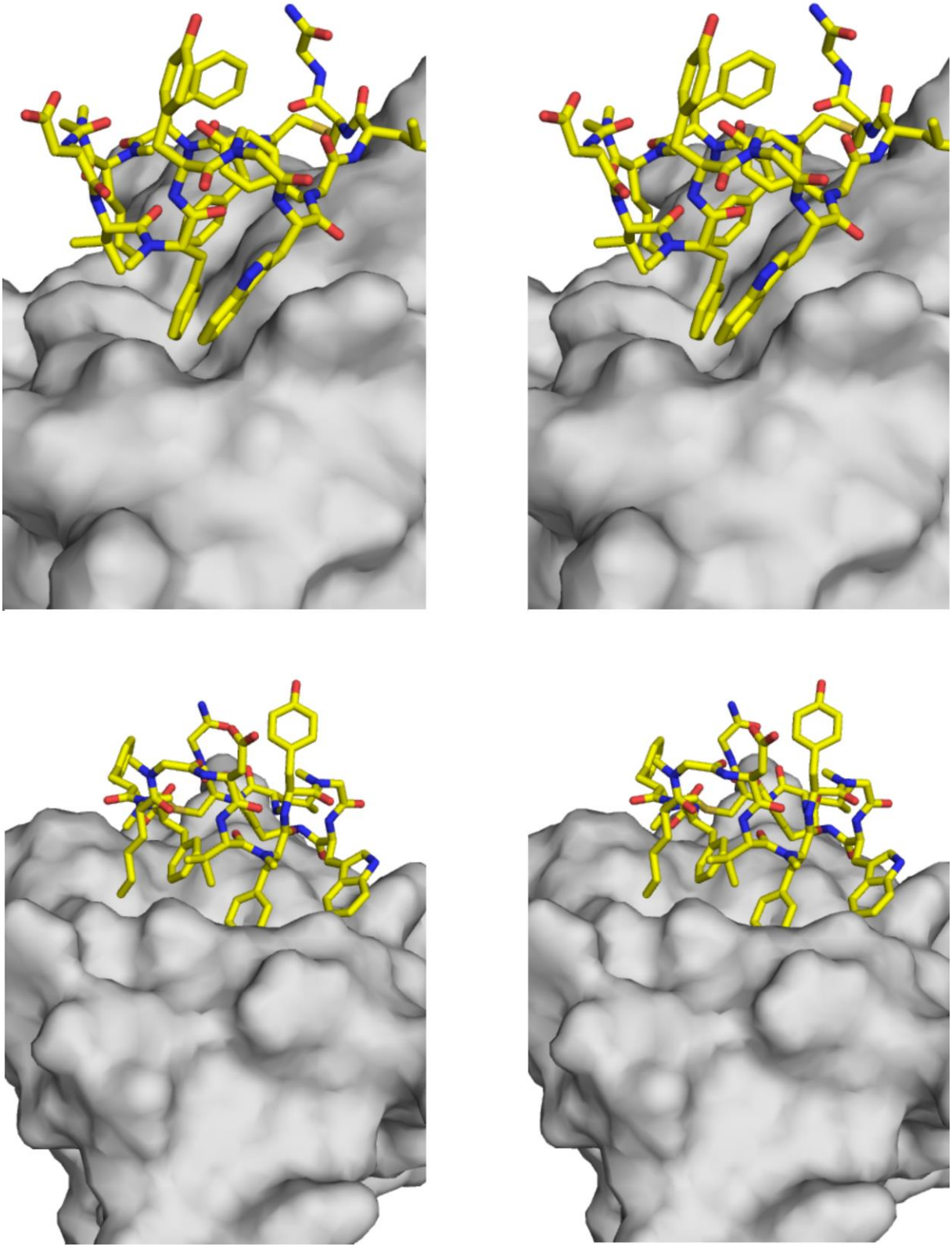

Figure S9. Hydrophobic sidechains of peptide-71 interact with the cleft of the PD-L1 protein (stereoview).

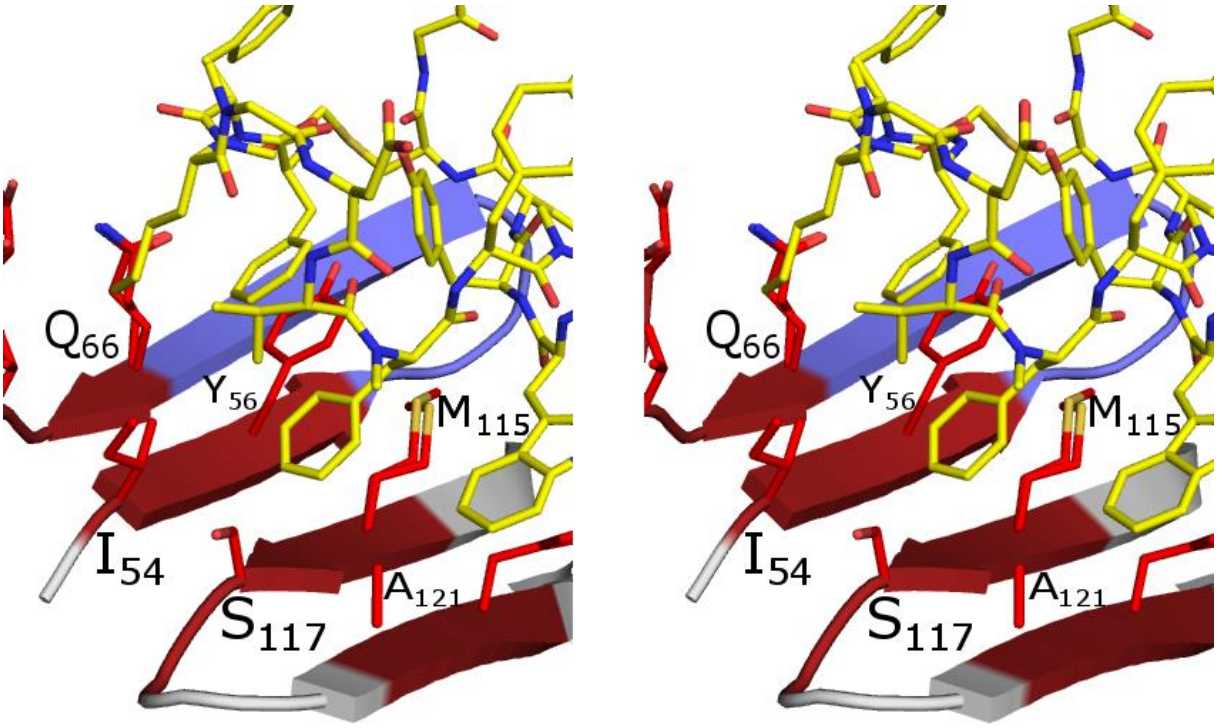

Figure S10. The stereoview close-up into the interaction surface in the PD-L1/peptide-71 complex. Hydrophobic surface of the interaction is presented in red, while hydrophilic in blue.

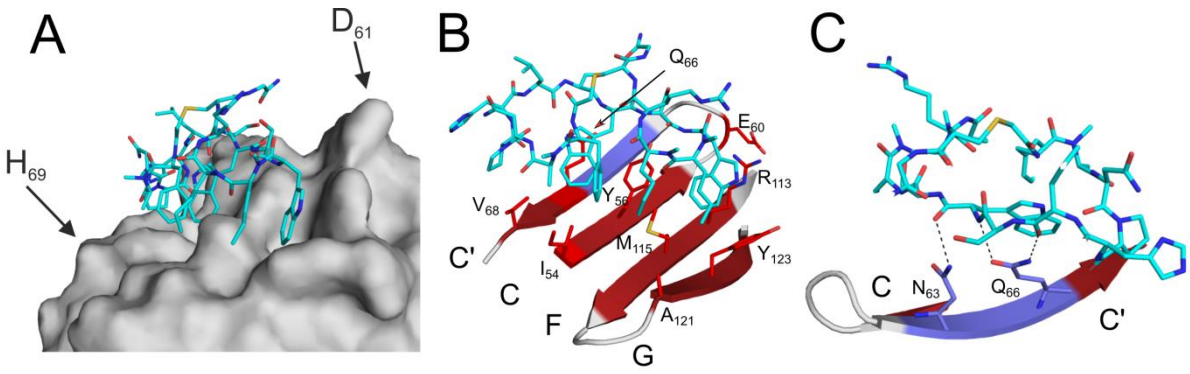

Figure S11. Detailed view into the PD-L1/peptide-57 interaction. A) Indole moieties interact with clefts characteristic for the “face-on” binding mode of macrocyclic peptides. B) Peptide-57 binds PD-L1 at the palm of the β-sheet composed of strands G, F, C and C’ mostly by hydrophobic interactions (red). C) The polar zone of the interaction surface includes three hydrogen bonds contributed by two backbones and one sidechain of amines of the peptide.

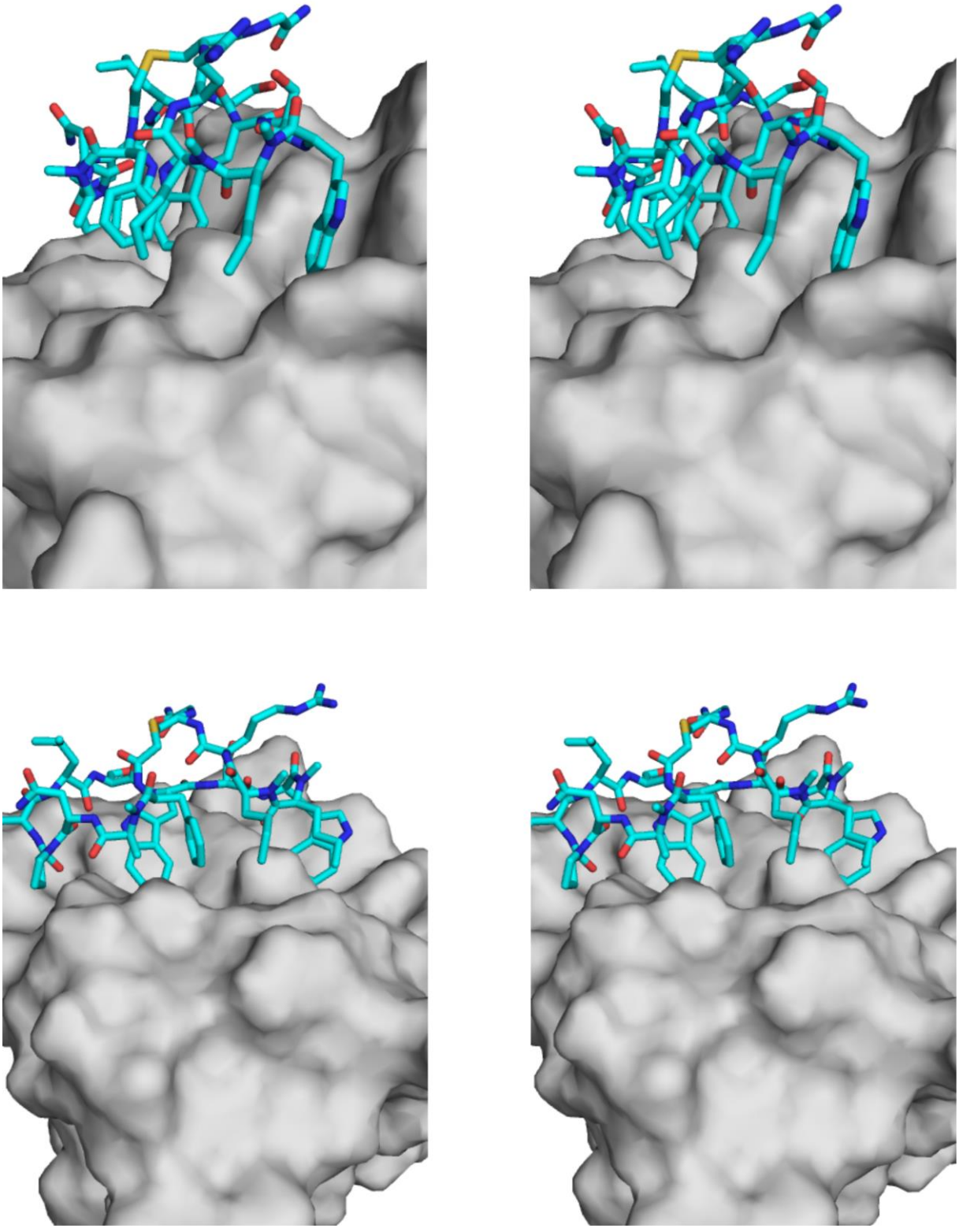

Figure S12. Hydrophobic side chains of peptide-57 interact with the cleft of PD-L1 protein (stereoview).

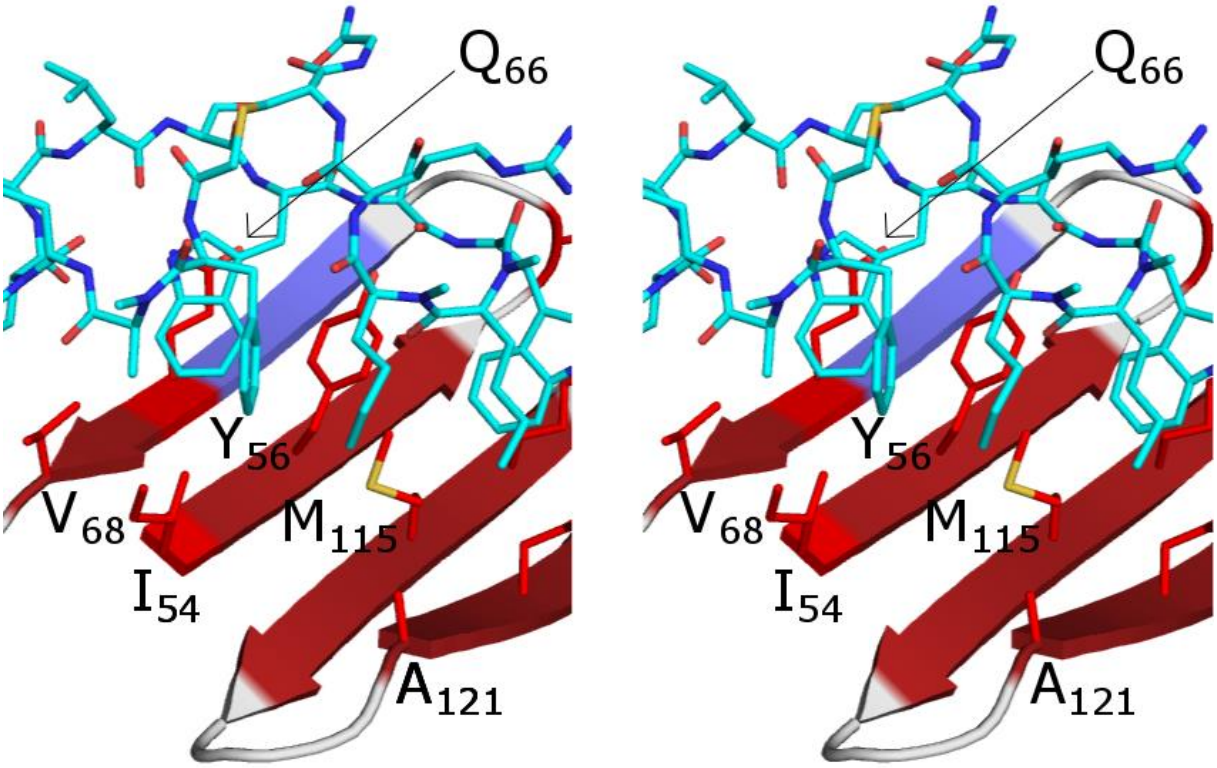

Figure S13. The stereoview close-up into the interaction surface in the PD-L1/peptide-57 complex. The hydrophobic surface of the interaction is shown in red while hydrophilic in blue.

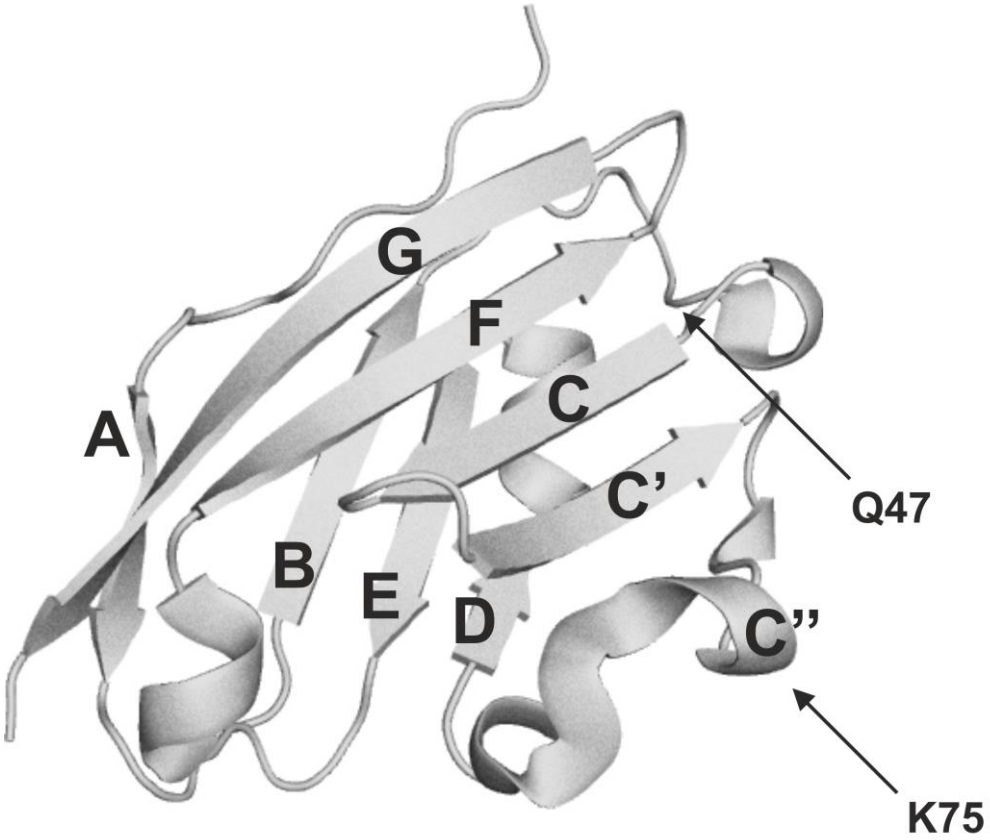

Figure S14. Canonical designation of strands and loops of extracellular domain of PD-L1.

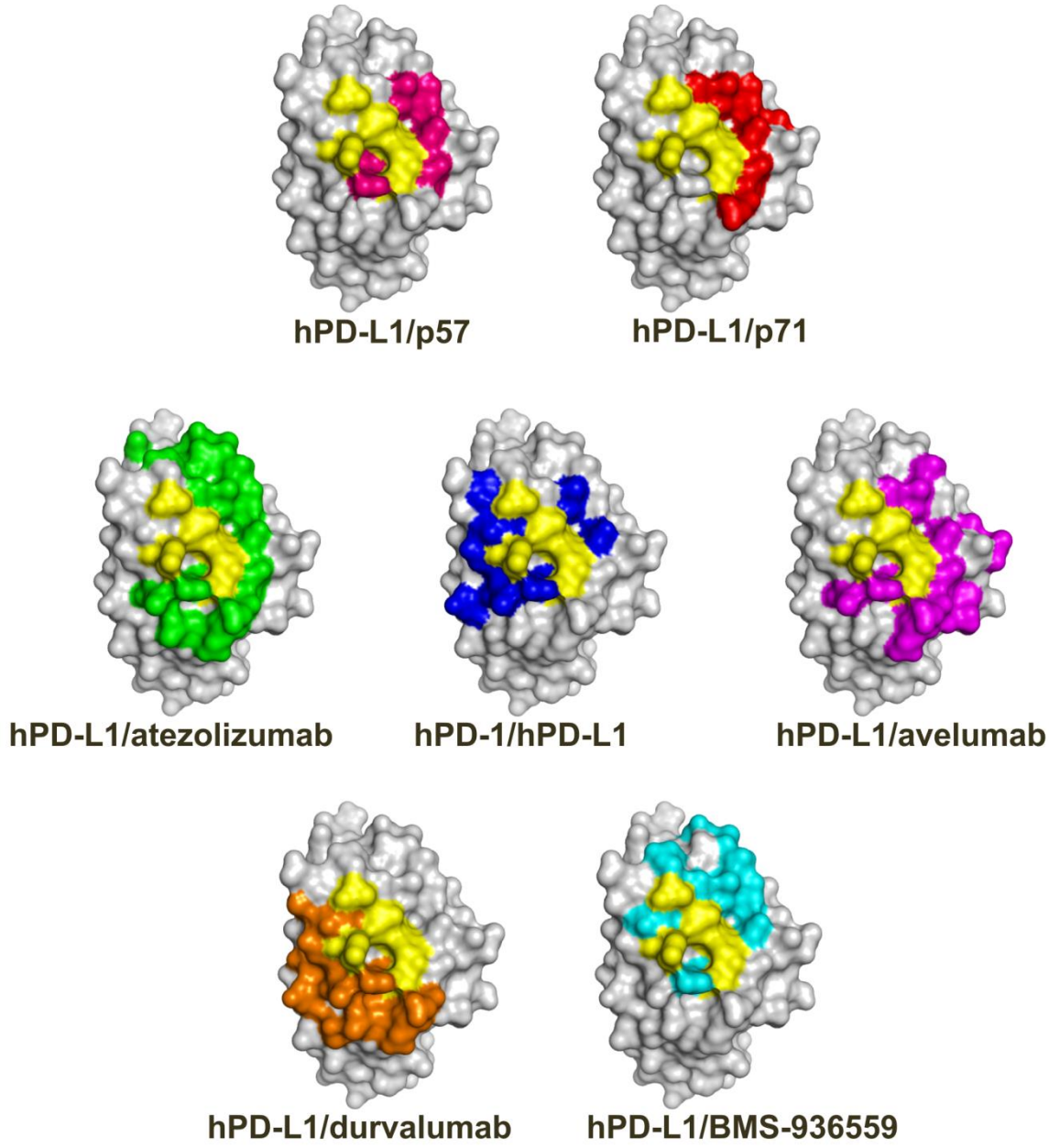

Figure S15. Interactions of PD-L1 with macrocyclic peptides and anti-PD-L1 antibodies. Upper panel: interaction interfaces of PD-L1 (surface representation) with peptides -57 (pink) and -71 (red) and shared regions targeted by the antibodies and the peptides are colored in yellow. Lower panels: The PD-L1 surface representation with the anti-PD-L1 antibodies (atezolizumab, avelumab, durvalumab, BMS-936559) and PD-1 receptor, the interaction surfaces colored green, magenta, orange, cyan and dark blue, respectively. The shared regions targeted by the peptides, the antibodies and PD-1 on the PD-L1 surface are presented in yellow.

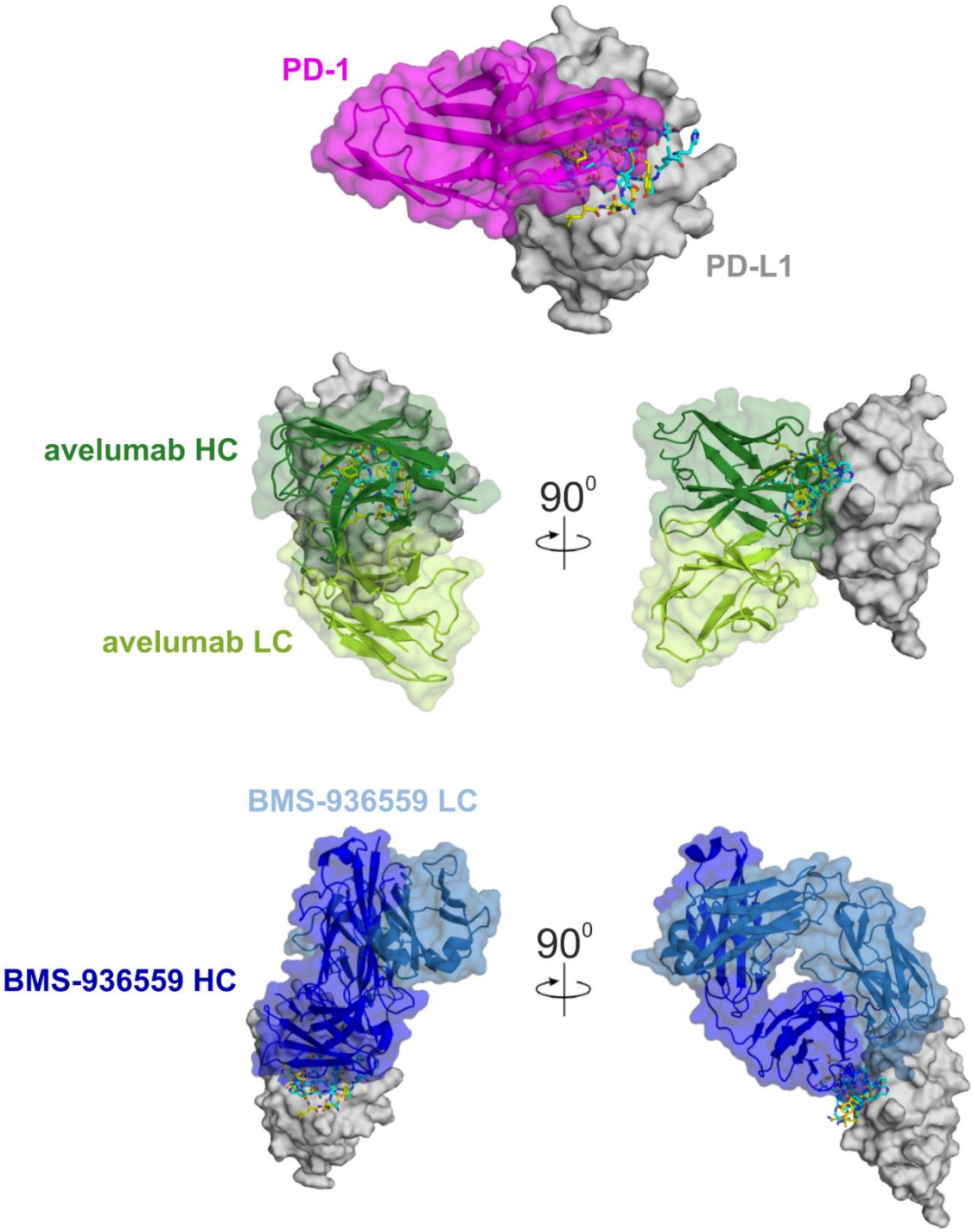

Figure S16. Comparison of the interface interactions of the PD-L1/antibodies and PD-L1/macrocyclic peptides complexes. Upper panel: the complexes of PD-1/PD-L1 and the peptides/PD-L1. Middle panel: comparison of the PD-L1/avelumab interactions to the PD-L1/peptide -57 and -71 interaction. Lower panel: comparison of the PD-L1/BMS-936559 interactions to the PD-L1/peptide -57 and -71 interactions.

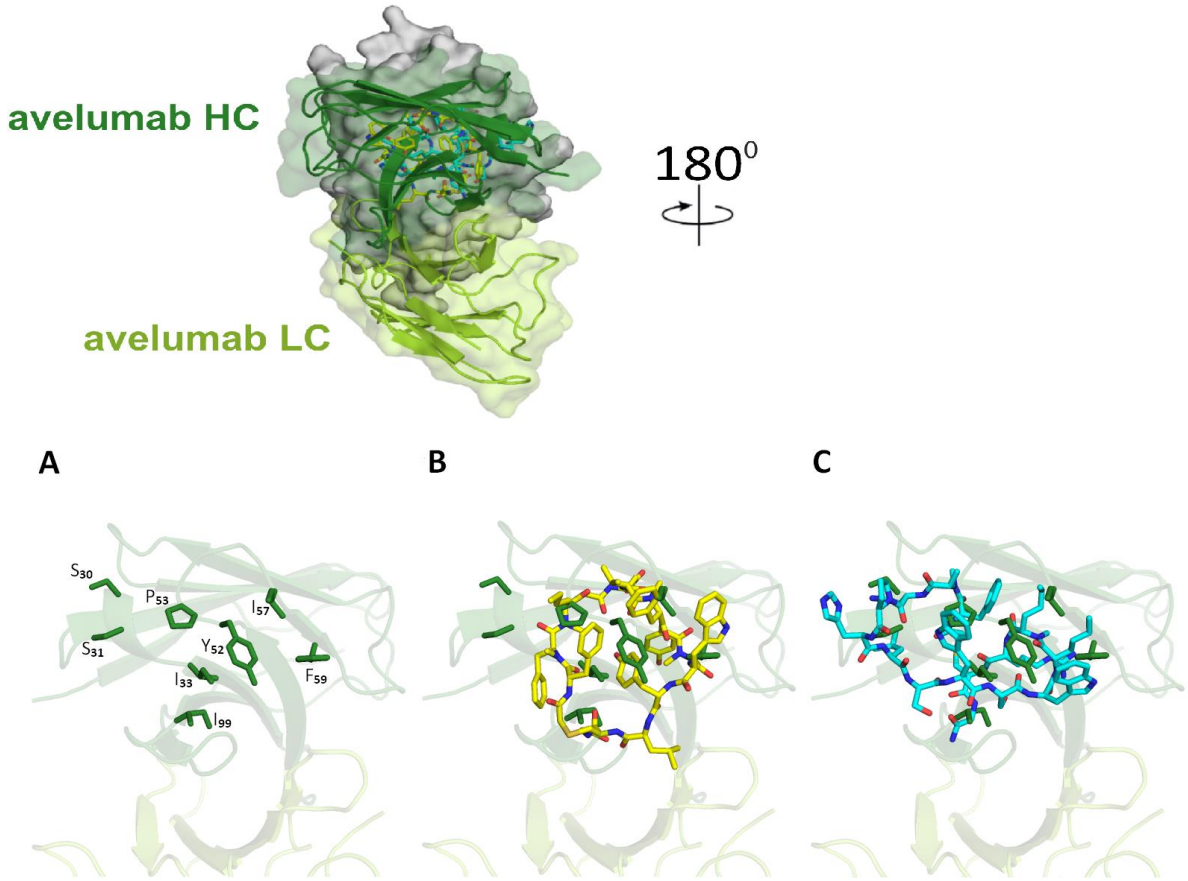

Figure S17. Comparison of interactions in the PD-L1/avelumab and PD-L1/peptides complexes. (A) The PD-L1/avelumab structure with highlighted side chains of the avelumab amino acids involved in the interaction with PD-L1 (PD-L1 not shown).. (B) The PD-L1/avelumab complex overlapped with the PD-L1/peptide-71 structure (PD-L1 not shown). (C) The PD-L1/avelumab complex overlapped with the PD-L1/peptide-57 structure (PD-L1 not shown).

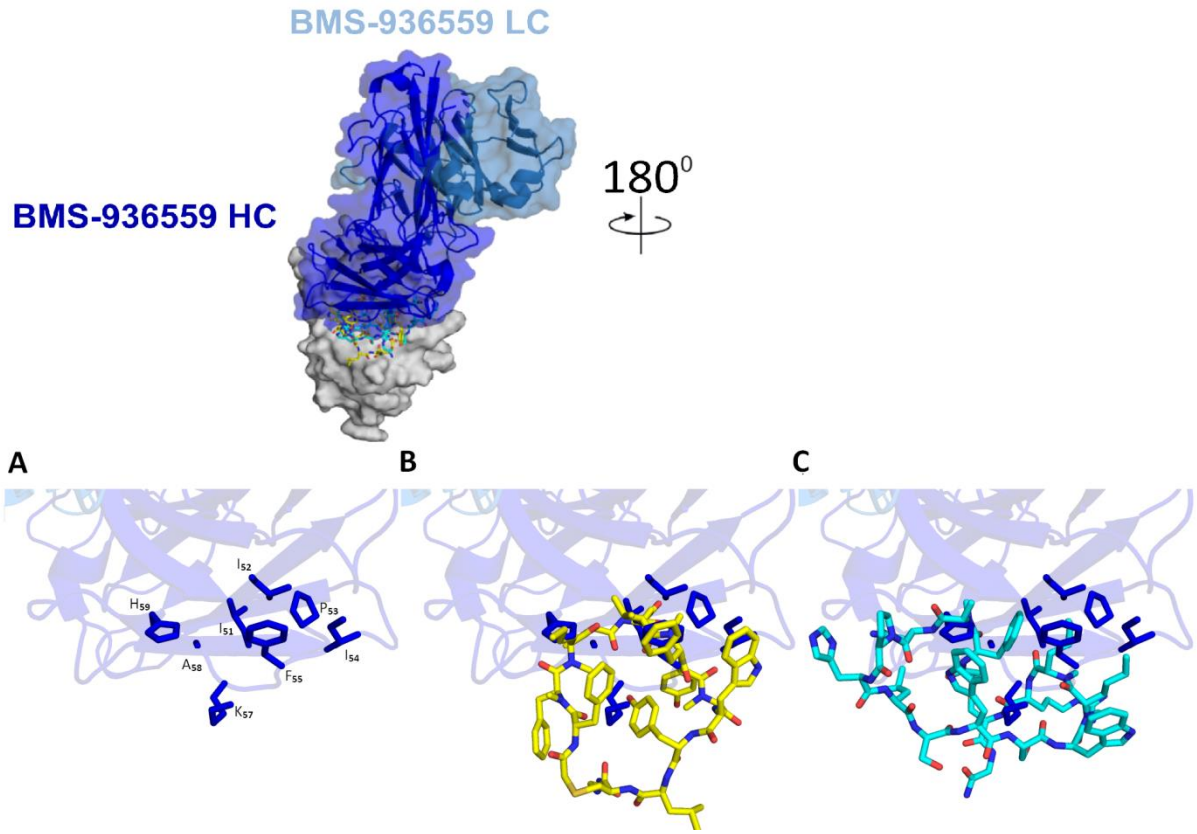

Figure S18. Comparison of the interactions in the PD-L1/ BMS-946559 and PD-L1/peptides complexes. (A) The PD-L1/ BMS-946559 structure with highlighted side chains of the BMS-946559 amino acids involved in the interaction with PD-L1 (PD-L1 not shown). (B) The PD-L1/ BMS-946559 complex overlapped with the PD-L1/peptide-71 structure (PD-L1 not shown). (C) The PD-L1/ BMS-946559 complex overlapped with the PD-L1/peptide-57 structure (PD-L1 not shown).

References

[1] K. M. Zak, P. Grudnik, K. Guzik, B. J. Zieba, B. Musielak, A. Dömling, G. Dubin, T. A. Holak, *Oncotarget* **2016**, *7*, 30323–35.

[2] F. H. Niesen, H. Berglund, M. Vedadi, *Nat. Protoc.* **2007**, *2*, 2212–2221.

[3] F. J. van Kuppeveld, J. T. van der Logt, A. F. Angulo, M. J. van Zoest, W. G. Quint, H. G. Niesters, J. M. Galama, W. J. Melchers, *Appl. Environ. Microbiol.* **1992**, *58*, 2606–15.

[4] U. Mueller, N. Darowski, M. R. Fuchs, R. Förster, M. Hellmig, K. S. Paithankar, S. Pühringer, M. Steffien, G. Zocher, M. S. Weiss, *J. Synchrotron Radiat.* **2012**, *19*, 442–449.

[5] P. Evans, *Acta Crystallogr. Sect. D Biol. Crystallogr.* **2006**, *62*, 72–82.

[6] W. Kabsch, *Acta Crystallogr. D. Biol. Crystallogr.* **2010**, *66*, 125–32.

[7] K. M. Sparta, M. Krug, U. Heinemann, U. Mueller, M. S. Weiss, *J. Appl. Crystallogr.* **2016**, *49*, 1085–1092.

[8] A. J. McCoy, R. W. Grosse-Kunstleve, P. D. Adams, M. D. Winn, L. C. Storoni, R. J. Read, *J. Appl. Crystallogr.* **2007**, *40*, 658–674.

[9] M. D. Winn, C. C. Ballard, K. D. Cowtan, E. J. Dodson, P. Emsley, P. R. Evans, R. M. Keegan, E. B. Krissinel, A. G. W. Leslie, A. McCoy, et al., *Acta Crystallogr. Sect. D Biol. Crystallogr.* **2011**, *67*, 235–242.

[10] P. Emsley, K. Cowtan, *Acta Crystallogr. Sect. D Biol. Crystallogr.* **2004**, *60*, 2126–2132.

[11] P. Emsley, B. Lohkamp, W. G. Scott, K. Cowtan, *Acta Crystallogr. Sect. D Biol.*

Crystallogr. **2010**, *66*, 486–501.

[12] G. N. Murshudov, P. Skubák, A. A. Lebedev, N. S. Pannu, R. A. Steiner, R. A. Nicholls, M. D. Winn, F. Long, A. A. Vagin, *Acta Crystallogr. Sect. D Biol. Crystallogr.* **2011**, *67*, 355–367.

[13] P. D. Adams, P. V. Afonine, G. Bunkóczi, V. B. Chen, I. W. Davis, N. Echols, J. J. Headd, L.-W. Hung, G. J. Kapral, R. W. Grosse-Kunstleve, et al., *Acta Crystallogr. Sect. D Biol. Crystallogr.* **2010**, *66*, 213–221.

[14] V. B. Chen, W. B. Arendall, J. J. Headd, D. A. Keedy, R. M. Immormino, G. J. Kapral, L. W. Murray, J. S. Richardson, D. C. Richardson, *Acta Crystallogr. D. Biol. Crystallogr.* **2010**, *66*, 12–21.

[15] E. A. Villar, D. Beglov, S. Chennamadhavuni, J. A. Porco, D. Kozakov, S. Vajda, A. Whitty, A. Whitty, *Nat. Chem. Biol.* **2014**, *10*, 723–31.

[16] X. Cheng, V. Veverka, A. Radhakrishnan, L. C. Waters, F. W. Muskett, S. H. Morgan, J. Huo, C. Yu, E. J. Evans, A. J. Leslie, et al., *J. Biol. Chem.* **2013**, *288*, 11771–11785.

[17] D. Y.-W. Lin, Y. Tanaka, M. Iwasaki, A. G. Gittis, H.-P. Su, B. Mikami, T. Okazaki, T. Honjo, N. Minato, D. N. Garboczi, *Proc. Natl. Acad. Sci. U. S. A.* **2008**, *105*, 3011–6.

[18] M. M. Miller, C. Mapelli, M. P. Allen, M. S. Bowshe, K. M. Boy, E. P. Gillis, D. R. Langley, E. Mull, M. A. Poirier, N. Sanghvi, L.-Q. Sun, D. J. Tenney, K.-S. Yeung,J. Zhu, P. C. Reid, P. M. Scola, L. A. Cornelius *Bristol-Myers Squibb Company; US 20140294898 A1* **2014**.

[19] S. Tan, H. Zhang, Y. Chai, H. Song, Z. Tong, Q. Wang, J. Qi, G. Wong, X. Zhu,

W. J. Liu, et al., *Nat. Commun.* **2017**, *8*, 14369.

[20] Z. Na, S. P. Yeo, S. R. Bharath, M. W. Bowler, E. Balıkçı, C.-I. Wang, H. Song, *Cell Res.* **2017**, *27*, 147–150.

[21] S. Tan, K. Liu, Y. Chai, C. W.-H. Zhang, S. Gao, G. F. Gao, J. Qi, *Protein Cell* **2017**, 1–5.

[22] K. Liu, S. Tan, Y. Chai, D. Chen, H. Song, C. W.-H. Zhang, Y. Shi, J. Liu, W. Tan, J. Lyu, et al., *Cell Res.* **2017**, *27*, 151–153.

Author contributions

K.M.M., K.M.Z., G.D. and T.A.H designed the research. K.M.M. performed the experiments, refined the structures, analyzed data and wrote the draft of the manuscript. P.G. collected X-ray data and solved structures. L.S. and J.K. performed cell experiments. E.R.S, Ł.B., T.Z.Z. and S.S. synthesized the compounds. K.M.Z. provided support with preparation of expression plasmids. B.M. performed NMR experiments. D.S. performed DSF experiments. G.D., A.D. and T.A.H. analyzed data and wrote the final version of the manuscript. All authors discussed the experiments and commented on the manuscript.